Rainbows: Mie computations and the Airy approximation

Ru T. Wang and H. C. van de Hulst

Efficient and accurate computation of the scattered intensity pattern by the Mie formulas is now feasible for size parameters up to $x = 50{,}000$ at least, which in visual light means spherical drops with diameters up to 6 mm. We present a method for evaluating the Mie coefficients from the ratios between Riccati-Bessel and Neumann functions of successive order. We probe the applicability of the Airy approximation, which we generalize to rainbows of arbitrary p (number of internal reflections $= p - 1$), by comparing the Mie and Airy intensity patterns. Millimeter size water drops show a match in all details, including the position and intensity of the supernumerary maxima and the polarization. A fairly good match is still seen for drops of 0.1 mm. A small spread in sizes helps to smooth out irrelevant detail. The dark band between the rainbows is used to test more subtle features. We conclude that this band contains not only externally reflected light ($p = 0$) but also a sizable contribution from the $p = 6$ and $p = 7$ rainbows, which shift rapidly with wavelength. The higher the refractive index, the closer both theories agree on the first primary rainbow ($p = 2$) peak for drop diameters as small as 0.02 mm. This may be useful in supporting experimental work.

I. Introduction

Can anything new be said about the rainbow? Yes. The insight that this phenomenon arises from the play of light in a single spherical drop is 7 centuries old, the full geometrical optics theory of Descartes 3-1/2 centuries, and its modification by Airy to take account of diffraction just 1-1/2 centuries. Exactly a century ago Lorenz,[1] and independently after that, Mie[2] and Debye[3] derived the rigorous analytic solution of the scattering of light by a homogeneous sphere of any size and refractive index. This infinite series, now generally called the Mie solution, should indeed include all there is to be said about the rainbow produced by a spherical water drop. Certain transformations of the Mie series, based on the pioneering work of Debye, lead indeed to the Airy formulas as was known half a century ago.[4] So the question is justified: what is new since then?

We feel excused from the duty to provide greater historical detail, for this can be found in excellent books[5] and papers.[6] Nor shall we enter into the fascinating aspects of the optical appearance of the rainbow in various natural circumstances. Papers by Fraser[7] and delightful books by Minnaert[8] and Greenler[9] explain many curious details.

So back to straight mathematical physics. When one of us reviewed the state of the art in 1957,[10] the conclusion was disappointing. A huge gap then existed between the relatively small sizes, where the Mie series was manageable, and the very large sizes, where the assumptions of the Airy theory were fulfilled. When the size parameter was written as

$$x = \frac{2\pi a}{\lambda}, \tag{1}$$

where $2a$ is the drop diameter and λ is the wavelength, the gap at that time was estimated to be between $x = 30$ and $x = 2000$. In this gap no practical method was available to compute a quantitatively reliable intensity pattern in the rainbow region.

Two successful moves to close this gap have been made since then. The first, Nussenzvieg's complex angular momentum theory,[11–13] extends the large drop theory to lower size parameters. It is based on a rigorous transformation of the Bessel functions in the Mie series and leads to a new series expansion which converges most rapidly if the drops are large. The Airy theory corresponds to the lowest-order approximation of this expansion. Nussenzveig's solution has been found reliable by comparison with straight numerical Mie computations. But the form remains rather complex and has not found extended use.

The second move closes the gap from the lower end.

When this work was started Ru Wang was with University of Florida, Space Astronomy Laboratory, Gainesville, Florida 32609; he is now with Institute for Space Science & Technology, Space Astronomy Laboratory, 1810 NW 6th Street, Gainesville, Florida 32609. H. C. van de Hulst is with Leiden Observatory, P.O. Box 9513, NL-2300 RA Leiden, The Netherlands.

Received 8 November 1989.
0003-6935/91/010106-12$05.00/0.

Stimulated by the pervasive needs for Mie computation many authors have developed codes efficient even at large size parameters. We show below that reliable Mie computations are now feasible up to $x = 50{,}000$ at least.

In Sec. II we explain our computational method, referring to Appendix A for the direct comparison with some other well-known algorithms. Section III summarizes the Airy approximation formulas which we found useful in discussing rainbows of arbitrary order, particle size, and refractive index, and compares the Mie and Airy profiles for the two classical rainbows. A special study of the dark band between these two main rainbows (Sec. IV) permits us to check some finer details. The extension to rainbows at different refractive indices and by smaller particles is made in Sec. V. Section VI contains the main conclusions.

II. Methods of Mie Computation

All researchers agree that the most difficult task in the Mie calculations is to find the partial wave coefficients. The nth pair of expansion coefficients of the field outside a homogeneous sphere is (notation from Ref. 10, p. 123)

$$a_n = [\psi_n'(y)\psi_n(x) - m\psi_n(y)\psi_n'(x)]/[\psi_n'(y)\zeta_n(x) - m\psi_n(y)\zeta_n'(x)],$$
$$b_n = [m\psi_n'(y)\psi_n(x) - \psi_n(y)\psi_n'(x)]/[m\psi_n'(y)\zeta_n(x) - \psi_n(y)\zeta_n'(x)]. \quad (2)$$

Here x is the real size parameter, m is the refractive index, which may be complex, and $y = mx$. The first requirement is to compute the nth-order Riccati-Bessel Neumann and Hankel functions ψ_n, χ_n, and ζ_n and their derivatives, of which ψ_n can have either a real argument x or a complex argument y. The Mie series with these accurately evaluated coefficients converge slowly. The total number of terms, $n_{\max}$, required for good convergence has in practice been found to be[14,15]

$$n_{\max} \sim x + 4x^{1/3} + 2. \quad (3)$$

Early workers, including the pioneers themselves, immediately noticed the arduous numerical problems for large x and evaded it by going to asymptotic expressions. Lorenz,[1] in particular, went as far as explaining the rainbows. In modern days a widespread method of calculating the ψ_n, χ_n, and ζ_n functions [summarily denoted by $F_n(z)$] and their derivatives is through the use of the recurrence formulas:

$$F_{n-1}(z) + F_{n+1}(z) = (2n+1)F_n(z)/z, \quad (3a)$$

$$F_n'(z) = -nF_n(z)/z + F_{n-1}(z). \quad (3b)$$

All F_n and F_n' functions here are simply related to the spherical Bessel, Neumann, or Hankel functions, e.g., $\psi_n(z) = zj_n(z)$, $\chi_n(z) = -zy_n(z)$, $\zeta_n(z) = zh_n^{(2)}(z)$, etc., which in turn are combinations of harmonic functions $\sin(lz)$ and $\cos(lz)$ where l runs from $l = 1$ to $l = n$. Equations (3a) and (3b) require a judicious use in either manual or machine computations, because errors or breakdowns may occur in computing $\sin(lz)$ and $\cos(lz)$ for large l and $|z|$ even when carrying a large number of digits. Many authors[14–23] have worked on the practical aspects of developing efficient Mie algorithms.

Our development of Mie algorithms since 1973 was first motivated by the necessity of absolute magnitude calibration of our microwave scattering measurements[24] and then by the wish to cover particle sizes either too large or too small for the experiment to simulate. Our preferred algorithm[25,26] is based on the ratio method. It evaluates all (a_n,b_n) terms via two precomputed arrays of ratios p_n and q_n between the Riccati-Bessel and Neumann functions of successive order. It provides numerical accuracy over wide ranges of x and m even with a modest number of digits carried in the computation and is also useful in computing the scattering by infinite cylinders. The accuracy and speed of this method are compared with three other well-known algorithms in Appendix A.

Dividing both sides of Eq. (3a) by $F_n(z)$ and rearranging terms, one obtains the recurrence formulas for the ratios

$$p_n(z) = \psi_n(z)/\psi_{n-1}(z) = 1/[(2n+1)/z - p_{n+1}(z)], \quad (4)$$

$$q_n(x) = \chi_n(x)/\chi_{n-1}(x) = (2n-1)/x - 1/q_{n-1}(x). \quad (5)$$

Although Eqs. (4) and (5) are mathematically the same formula, they are written separately to emphasize that a downward recurrence must be employed to generate by Eq. (4) the $p_n(z)$ array, whose argument z can be either real or complex, while an upward recurrence must be used to obtain by Eq. (5) the $q_n(x)$ array which has only a real argument x in a sphere problem. For example, starting from a sufficiently large order N and taking the asymptotic value

$$p_{N+1}(z) \sim z/(2N+3) \quad (6)$$

as the starting value, the successive downward elements $p_N,p_{N-1},\ldots,p_2,p_1$ are computed by (4). Our current best choice for N, valid for all sphere sizes, is

$$N = 1.1|z| + 10. \quad \text{if } |z| \le 10000,$$
$$N = 1.01|z| + 10. \quad \text{if } |z| > 10000. \quad (7)$$

The $q_n(x)$ array is computed by Eq. (5) upward from $q_1(x) = 1/x + \tan x$ to $n = n_{\max}$. We note, however, that equally accurate and faster $\chi_n(x),\chi_n'(x)$ upward recurrence calculations by Eqs. (3a) and (3b), than through Eq. (5), are employed in many of our recent routines. When these ratio arrays have been completed, all ψ_n, χ_n functions for $n > 1$ are obtained by successive multiplications from the $n = 1$ functions ψ_1 and χ_1 through the ratio arrays. Similarly, all derivatives needed in Eq. (2) can also be evaluated from p_n, q_n arrays alone, for from Eq. (3b) we find that two additional ratios commonly known as the logarithmic derivatives are given by

$$A_n(z) = \psi_n'(z)/\psi_n(z) = -n/z + 1/p_n(z), \quad (8)$$

$$B_n(x) = \chi_n'(x)/\chi_n(x) = -n/x + 1/q_n(x). \quad (9)$$

The Mie coefficients [Eq. (2)] can now be rewritten in a form convenient for computation:

$$a_n = 1/(1 + i\chi_n(x)[A_n(y) - mB_n(x)]/\{\psi_n(x)[A_n(y) - mA_n(x)]\}),$$
$$b_n = 1/(1 + i\chi_n(x)[mA_n(y) - B_n(x)]/\{\psi_n(x)[mA_n(y) - A_n(x)]\}), \quad (10)$$

where

$$\psi_n(x) = \psi_1(x) \prod_{i=2}^{n} p_i(x),$$

$$\chi_n(x) = \chi_1(x) \prod_{i=2}^{n} q_i(x), \quad \text{for } n \geq 2 \quad (11)$$

$$\psi_1(x) = \sin x/x - \cos x; \quad \chi_1(x) = \cos x/x + \sin x, \quad \text{for } n = 1. \quad (12)$$

Evaluation of all Mie coefficient pairs (a_n,b_n) is thus reduced to finding the simple ratio arrays $p_n(z)$, $A_n(z)$, $q_n(x)$, and $B_n(x)$, plus only two transcendental functions $\sin x$ and $\cos x$ in Eq. (12). The highest term n_{max}, with which we terminate a Mie series summation, is currently judged by

$$(|a_n|^2 + |b_n|^2)/(|a_1|^2 + |b_1|^2) \lesssim 10^{-14} \quad \text{at } n = n_{max}. \quad (13)$$

This has been noted to be consistent with the widely accepted criterion [Eq. (3)]. It should be recalled that, if one computes a Mie series beyond necessity ($n \gg n_{max}$), the series may become oscillatory or even divergent.[25]

In the Rayleigh region where x is very small, we modified the ratio method only by employing the direct expansion

$$\psi_1(x) \sim \sum_{n=1}^{4} (-1)^{n+1} x^{2n} \frac{2n}{(2n+1)!}, \quad (14)$$

which permitted accurate Mie calculation down to $x \sim 10^{-5}$.

Some properties of the ratios $p_n(y)$ and $A_n(y)$ are illustrated in Fig. 1, where the real and imaginary parts of the ratios are plotted for a fixed $x = 62$ against n from $n = 1$ to the Mie series termination $n_{max} = 79$. Figures 1(a) and (b) are for complex arguments $y = mx$, while Fig. 1(c) is for a real argument. These ratios were computed straight from Eqs. (4) and (8), i.e., without recourse to error prone Bessel function evaluations (Ref. 19, p. 20). Typically, for sufficient absorption the ratios form smoother curves and stay <1 in absolute value, thereby making the ratio method quite stable. For real arguments the $\psi_n(x)$ and $\psi_n'(x)$ are known to oscillate through positive and negative values many times before reaching their exponentially decaying tails at $n > x$. Here the ratios $p_n(x)$ and $A_n(x)$ are not bounded, but, except for the rare chance for one n where $\psi_n(x)$ may be very close to zero, the ratio method is still quite useful. The stability is such that only a modest number of digits is required for computing the ratios, which makes the method an efficient one at large x or y.

With the (a_n,b_n) terms computed, the angular distribution of scattered light is expressed by the following formulas[10,14,16,18,19]:

$$S_1(\theta) = \sum_{n=1}^{n_{max}} \frac{2n+1}{n(n+1)} [a_n\pi_n(\mu) + b_n\tau_n(\mu)],$$
$$S_2(\theta) = \sum_{n=1}^{n_{max}} \frac{2n+1}{n(n+1)} [a_n\tau_n(\mu) + b_n\pi_n(\mu)]. \quad (15)$$

$S_1(\theta)$ and $S_2(\theta)$ are the perpendicular and parallel scattering amplitude (complex) components at a scattering angle θ with respect to the plane: source–particle–observer, $\mu = \cos\theta$, $\pi_n(\mu) = dP_n(\mu)/d\mu$, $\tau_n(\mu) = \mu\pi_n(\mu) - (1 - \mu^2)d\pi_n(\mu)/d\mu$, and $P_n(\mu)$ is the nth order Legendre polynomial of μ. The corresponding scattering intensity components are

$$i_1(\theta) = |S_1(\theta)|^2, \quad i_2(\theta) = |S_2(\theta|^2. \quad (16)$$

The total scattering intensity for unpolarized incident light, $(S_{11})_{Mie}$ (the 1,1 element of the Muller scattering matrix), and the degree of linear polarization, $(P)_{Mie}$, are defined as

$$(S_{11})_{Mie} = (i_1 + i_2)/2, \quad (P)_{Mie} = (i_1 - i_2)/(i_1 + i_2). \quad (17)$$

The values of $(S_{11})_{Mie}$ are shown in Figs. 2–5 and 7, and $(P)_{Mie}$ is shown in Fig. 5 of this paper. Computation of the (π_n,τ_n) functions is much more straightforward than evaluating (a_n,b_n), and we employed the upward recurrence formulas given in the above literature.[10,14,16,18,19] A device to speed up the computation of the angular distribution, the use of a vector structured algorithm,[15] has not yet been tried.

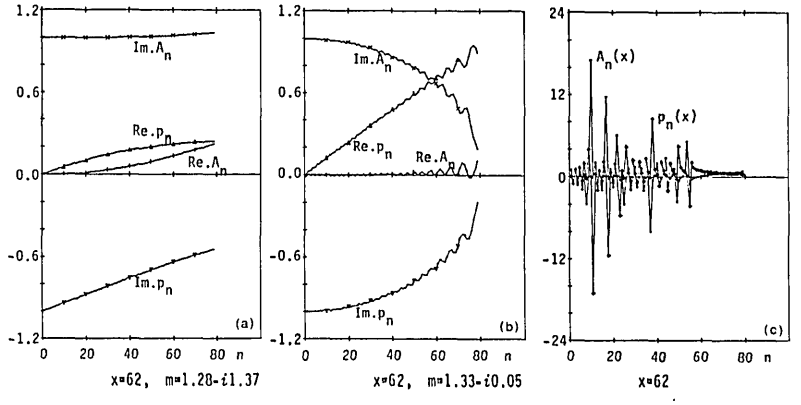

Fig. 1. Real and imaginary parts of the ratios $p_n(z)$ and $A_n(z)$ vs n for Riccati-Bessel function.

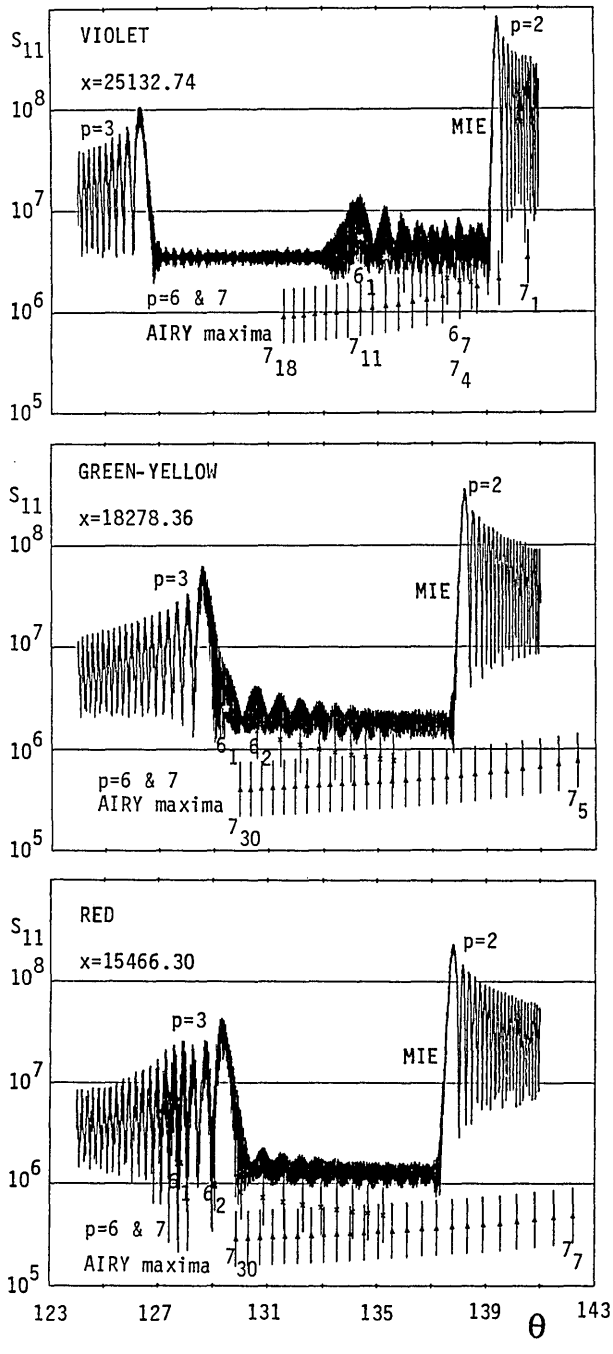

Fig. 2. Mie rainbow intensity profiles for a $2a = 3.2$-mm water drop at three visible wavelengths. Positions and intensities of the Airy maxima for the $p = 6$ and 7 rainbows are also shown.

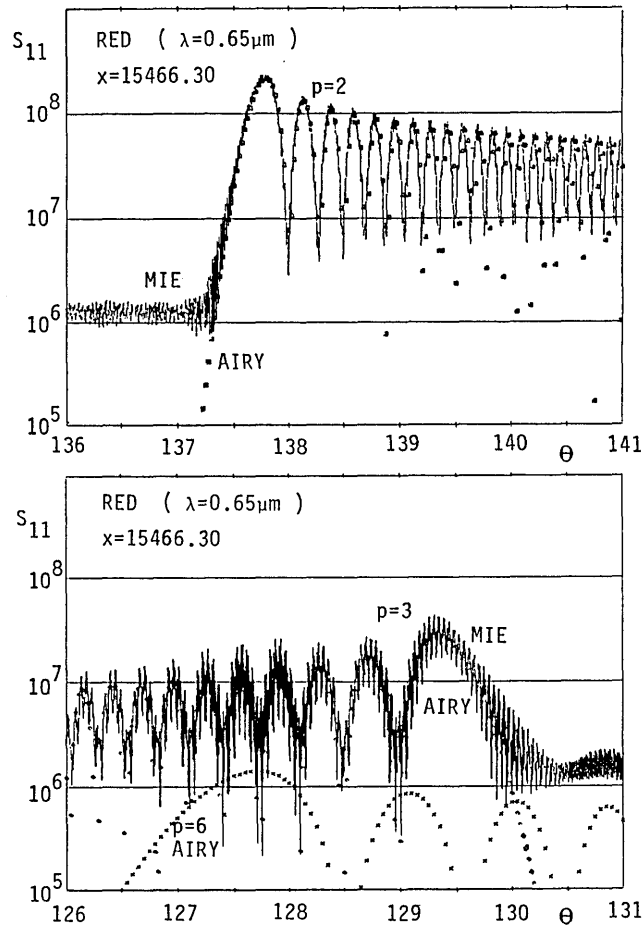

Fig. 3. Bottom of Fig. 2 is expanded separately for the primary (top) and secondary (bottom) rainbows. Airy intensity profiles for $p = 2$, 3, and 6 rainbows are also shown.

III. Airy Approximation and the Two Main Rainbows

It has been known since Descartes that the two main rainbows represent extrema occurring in the deviation angle of geometrical optics rays which have suffered one or two internal reflections in the drop. The bright sides flare in opposite directions so that a relatively dark band is left between the two rainbows. Since Young and Airy[27] we know that, upon taking diffraction into account, the infinite intensity at the extreme deviation angle is softened into a finite peak near, but not at, that angle and that the bright flare breaks up into separate maxima called supernumerary bows.

This entire theory is strictly asymptotic, i.e., valid for drops very much larger than the wavelength. In this section and in Sec. V we ask the simple questions: Do straight Mie computations show quantitative agreement with the asymptotic theory and at what particle size do deviations become visible?

We first recall the necessary equations from the Airy theory, which we formulate for raindows of arbitrary order, where p is the number of chords the ray has traveled through the particle and $p - 1$ is the number of internal reflections it has suffered.[28]

Let τ and τ' be the complements of incident and refraction angles of an incident ray; τ varies from $\pi/2$ for central incidence to 0 for incidence at the edge. After $p - 1$ internal reflections, the ray exits from the particle with a total deviation of $\theta = 2(\tau - p\tau')$. The corresponding rainbow angle $\theta_0(p,m)$ by geometrical optics (GO) is found from

$$\theta = 2\pi l + q\theta_0(p,m) = 2(\tau_p - p\tau_p'), \tag{18}$$

where l is an integer and $q = +1$ or $q = -1$ to define θ_0 in $0 < \theta_0 < \pi$, and where[29]

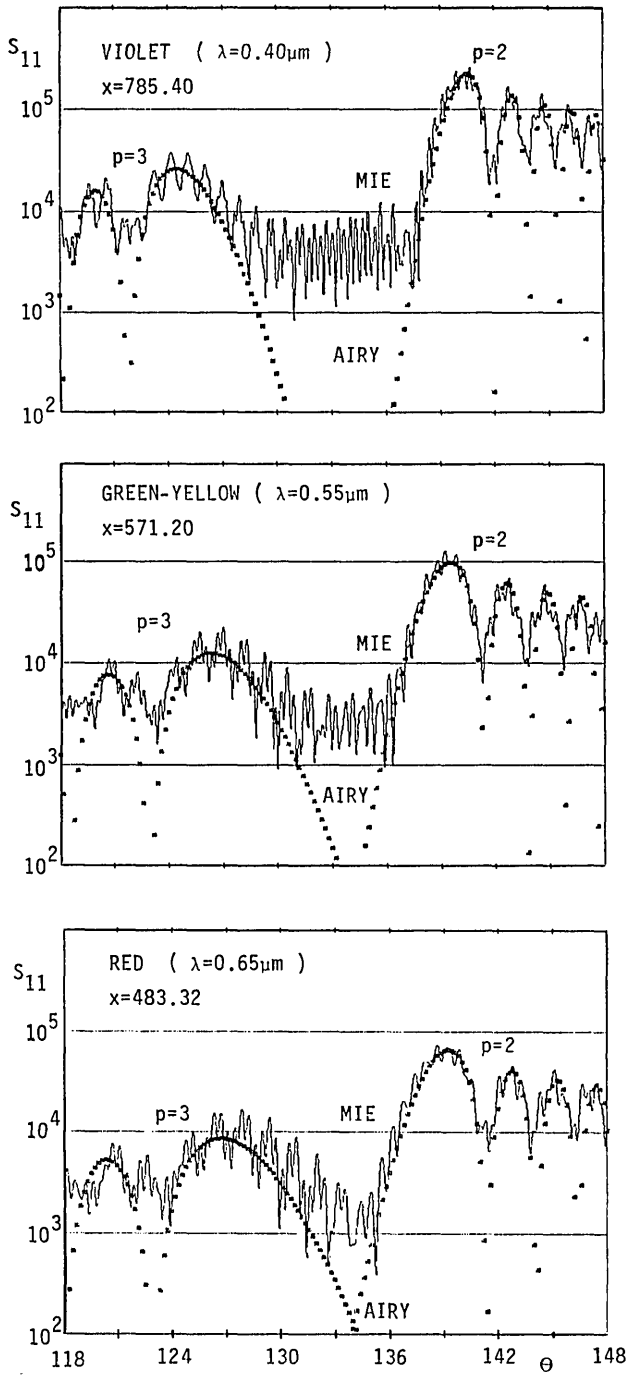

Fig. 4. Mie and Airy rainbow intensity profiles for a $2a = 0.1$-mm water drop at three visble wavelengths.

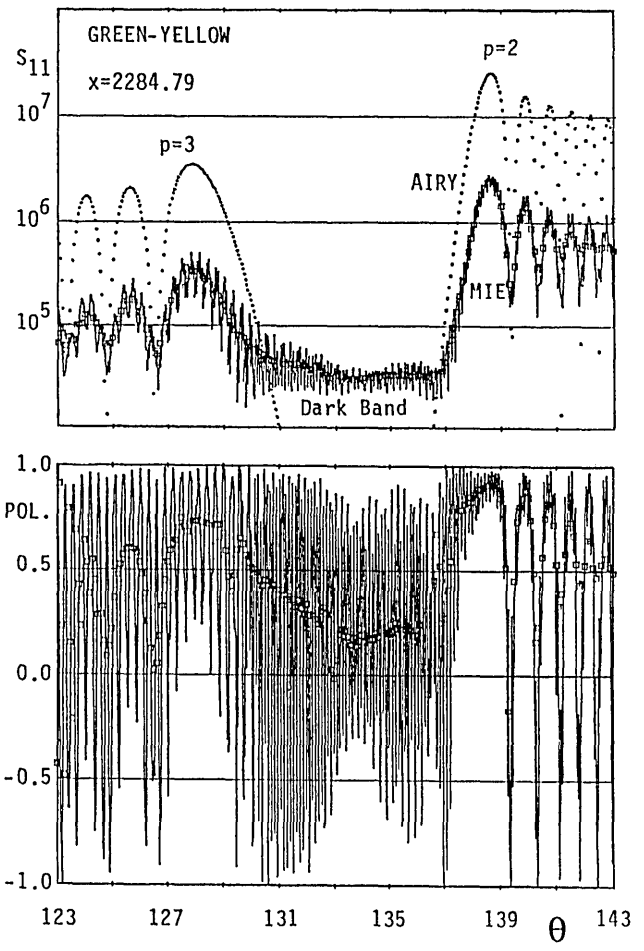

Fig. 5. Rainbow intensity (upper figure) and polarization (lower figure) profiles for a $2a = 0.4$-mm water drop. The $(S_{11})_{\text{Airy}}$ term is plotted a decade higher for readability. Mie profiles are plotted by continuous curves for the single size and are marked by a □ for the gamma size distribution.

$$\tan\tau_p = [(m^2-1)/(p^2-m^2)]^{1/2}, \tag{19}$$

$$\tan\tau_p' = [p^2(m^2-1)/(p^2-m^2)]^{1/2}. \tag{20}$$

Whenever $q = -1$, as it is for the primary rainbow, $\theta_0(p,m)$ is a minimum; for $q = 1$ it is a maximum. The rainbow forming rays for higher p strike closer to the droplet edge.

The explicit expression for $(S_{11})_{\text{Airy}}$, the total scattering intensity for unpolarized incident light, applicable to arbitrary p, m, and x, can be derived by extending that by van de Hulst for $p = 2$, polarization 1, and $m = 4/3$ (Ref. 10, p. 246, note an error: the numerical factor of 2.85 should be corrected to read 0.280):

$$(S_{11})_{\text{Airy}} = (\epsilon_1^2 + \epsilon_2^2)[81/(16\pi^2 h^4)]^{1/6} \times \cos\tau_p x^{7/3} f^2(z)/\sin\theta_0(p,m), \tag{21}$$

where $f(z)$ is the well-known Airy integral:

$$f(z) = \int_0^\infty \cos[\pi(zt - t^3)/2]dt. \tag{22}$$

The variables and parameters in Eqs. (21) and (22) are defined through the scattering geometry (Ref. 10, pp. 204 and 243–245 and Ref. 29, p. 470) by

$$\begin{aligned} z &= (-q)[12/(h\pi^2)]^{1/3} x^{2/3}(\theta - \theta_0); \\ h &= \{(p^2-1)^2/[p^2(m^2-1)]\} \cdot [(p^2-m^2)/(m^2-1)]^{1/2}; \\ \epsilon_i &= (1 - r_i^2)(r_i)^{(p-1)}, \qquad i = 1 \text{ or } 2 \text{ and } p \geq 2; \\ r_1 &= \sin(\tau_p - \tau_p')/\sin(\tau_p + \tau_p'); \quad r_2 = \tan(\tau_p - \tau_p')/\tan(\tau_p + \tau_p'). \end{aligned} \tag{23}$$

Here h gives the curvature of the cubic wavefront for

rainbow rays of order $p-1$. The front is more strongly curved for higher p and for smaller x. Consequently, the angular spacing between two successive supernumerary peaks becomes wider as p increases and/or x decreases. The Fresnel reflection coefficients r_1 and r_2, for polarizations 1 and 2, respectively, enter the Airy intensity through the factor $\epsilon_1^2 + \epsilon_2^2$ in Eq. (21). They are customarily taken constant and equal to their values at the GO rainbow ray. The size dependence of the rainbow peak intensity of $\sim x^{7/3}$ in Eq. (21) agrees with the size dependence in amplitude of $\sim x^{7/6}$ in Eq. (2.4) of Refs. 13 (β is our x). Nussenzveig's comment (i) to this factor might convey the impression that the advanced theory deviates progressively by an enhancement factor of $x^{1/6}$ (in amplitude) from the Airy theory. This is not the case. Instead, if θ_0 is the rainbow angle by GO, the main Airy peak and each supernumerary peak changes position as $(\theta - \theta_0) \sim x^{-2/3}$. Since, in the absence of any diffraction effects, the GO intensity near the divergence point is $(\theta - \theta_0)^{-1/2}$, this immediately explains why the intensity is enhanced as $x^{+1/3}$.

To evaluate and display the results obtained by Eq. (21) routinely via our VAX 11/750 and PDP 11/23 computers, we checked whether the accuracy of calculating Eq. (22) agreed with that given by Abramowitz and Stegun (Ref. 30, Sec. 10.4). The power series expansion of $f(z)$ was found appropriate for $|z| < 8$ and the asymptotic formulas were used for $|z| > 8$. We further note that the positions of Airy intensity maxima and minima can also be found rather closely without evaluating [Eq. (21)]. For the Airy supernumerary maxima ($K \geq 1$), the expression is (Ref. 10, p. 245)

$$|\theta_{\max,K} - \theta_0(p,m)| = h^{1/3}[3\pi(K + 1/4)/2]^{2/3}x^{-2/3}. \quad (24a)$$

To avoid an overestimate of ~9% on the left-hand side by putting $K = 0$ in Eq. (24a), the following correct formula is used only for the first Airy peak:

$$|\theta_{\max,0} - \theta_0(p,m)| = 1.087376(h\pi^2/12)^{1/3}x^{-2/3} \quad (24b)$$

For all Airy minima ($K \geq 0$), on the other hand,

$$|\theta_{\min,K} - \theta_0(p,m)| = h^{1/3}[3\pi(K + 3/4)/2]^{2/3}x^{-2/3}. \quad (24c)$$

Although the Airy theory has been discussed or modified in several ways in many rainbow articles to date,[6,10,13,29,31–33] direct comparisons with exact results from the Lorenz-Mie equations are scarce.[33] This may be due to the relatively recent availability of dependable Mie computer codes for large size parameters.[34,35] We now discuss a few graphic comparisons between the Mie and Airy results, as selected from a large body of water drops in the 0.0125–6.4-mm diam range and with refractive indices[36] $m = 1.331 - i1.3E\text{-}8$ at $\lambda = 0.65$ μm (red), $m = 1.334 - i1.5E\text{-}9$ at 0.55 μm (green-yellow), and $m = 1.343 - i3E\text{-}9$ at 0.40 μm (violet). In the Airy computations we neglected the imaginary part of the refractive index. We assume both the point light source and the observer are located far from the particle.

Figure 2 shows the Mie intensity, both polarizations added, at the three selected wavelengths for a drop with 3.2-mm diameter. Note, however, that such a large drop would not keep a perfect spherical shape in the atmosphere. The primary rainbow ($p = 2$) is seen at the right, and the secondary rainbow ($p = 3$) at the left. We return in Sec. IV to what happens in the dark band between these rainbows. The bottom figure in Fig. 2 is expanded in Fig. 3 to facilitate detailed Mie-Airy comparisons. Figures 2 and 3, and many others on a larger scale which we cannot reproduce, show the following features, familiar from classical rainbow theory:

The primary rainbow is ~7.7 (red) to 8.4 (violet) times more intense than the secondary rainbow.

All Airy maxima up to ~ the tenth supernumerary bow are at the predicted angles and have the right intensity.

The rainbows move closer together if we move from violet to red. The shift in the $p = 3$ rainbow is twice that in the $p = 2$ rainbow.

Altogether, at this size excellent agreement between Mie and Airy theories exists.

In contrast, the Mie and Airy intensities scattered by a drop of 0.1-mm diameter are depicted in Fig. 4. Overall agreement between the two for the first maxima at both sides ($p = 2$ and $p = 3$) is still surprisingly good. However, the size has become too small to trace the origin of all the wiggles. The dark band is still seen in the violet but diminishes in the red. The Airy theory predicts slightly larger shifts in the higher supernumerary bow positions for $p = 2$ than the Mie theory shown, and even more so for $p = 3$. What happens to still smaller drops is discussed in Sec. V.

To illustrate some finer details in Fig. 5 we present a similar graph for a drop with the intermediate size of $2a = 0.4$ mm at one wavelength. The intensities by Airy theory have been offset by a factor of 10 for better readability. The positions and intensities still match quite well. Also included in the top part of Fig. 5 is $(S_{11})_{\text{Mie}}$ for a very narrow size distribution of water droplets according to the Hansen-Travis standard gamma size distribution[37] with $b = 0.005$. The spread in drop sizes causes most wiggles in the intensity to be smoothed out. This gives an even better match with the Airy pattern at both main peaks ($p = 2$ and $p = 3$), but gives more smeared-out profiles for the second and higher supernumeraries. The bottom part of Fig. 5 shows the degree of polarization. For strictly one size this fluctuates. However, introducing the spread in sizes reveals a more regular curve. The polarization then remains positive over most of the range.

As a technical detail we note that the integration over x required to introduce the spread in sizes is in practice replaced by a summation, in which the limits x_1 and x_2 and the interval Δx may be chosen to fit convenience. In computing Fig. 5 we used $b = 0.005$, $x_e = 2285$, $x_1 = 0.71\ x_e$, and $x_2 = 1.32\ x_e$, placing these limits where the distribution function has gone down by 4 orders of magnitude. In addition we used $\Delta x = (x_2 - x_1)/40 = 35$ which, as shown by Dave[38] and pointed out to us by J. F. de Haan of the Free University, The Netherlands, is altogether too coarse to follow the individual wiggles. Consequently, the size averaged points in Fig. 5 may not be individually reliable.

Nevertheless, regarding the wiggles as quasistatistical fluctuations, it can be readily shown that the averages should have a random error ~4 times smaller than the original points, which explains the smoothing effect shown in Fig. 5.

Throughout the two main rainbows, $(P)_{\text{Mie}}$ is in perfect phase with $(S_{11})_{\text{Mie}}$, i.e., the higher the rainbow intensity the more strongly polarized is the rainbow light along the arc of the rainbow which is perpendicular to the scattering plane: sun–droplet–observer. Conversely, the lower the $(S_{11})_{\text{Mie}}$ the more competition is seen from light polarized parallel to the scattering plane. The strong polarization is caused by the fact that the ϵ_2 is very small because τ is close to the Brewster angle. Indeed, the Airy theory can be refined by taking the variation in magnitude and sign of ϵ_2 into account.

IV. Dark Band Between the Two Main Rainbows

The dark space separating the two main rainbows was undoubtedly noticed by careful observers of all times. It is named Alexander's dark band[6] in honor of Alexander of Aphrodisias (~200 A.D.). The low intensity level in this band also offers an opportunity to check whether the minor components of ray optics are rendered correctly by the Mie computation. Geometrical optics contributions from the $p = 1$, 2, and 3 rays are absent at these angles and the contributions by the $p = 4$ and $p = 5$ rays are very faint. Hence we expected that in the limit of large x the externally reflected ray ($p = 0$) would fully dominate. The intensity at $\theta = 132.5°$ in the GO limit for $m = 4/3$ (Ref. 10, p. 232) was calculated to be $(\bar{S}_{11})_{p=0} = 0.00525\,x^2$ and the degree of polarization is $(\bar{P})_{p=0} = 0.262$.

In Fig. 6 we have averaged the intensity and polarization over the arbitrarily chosen interval $131° \le \theta \le 134°$ in the dark band for each drop size for which exact Mie computations were made. The graphs approach the $p = 0$ limits for large x fairly well but not quite. Moreover, the points for the individual wavelengths show puzzling jumps of several percent. Figure 2, already presented above, shows what actually happens. Two further rainbows with typical Airy patterns lurk inside the dark band.[34,39] The strongest one is the $p = 6$ rainbow caused by five internal reflections. Its head moves rapidly with wavelength: in the violet, it is just at the edge of the chosen test interval; in the yellow-green, it has moved beyond the other edge; and in the red, it is submerged under the $p = 3$ bow. The fainter $p = 7$ rainbow moves in the opposite direction. Its contribution is just visible in the violet because it is partly free from the $p = 6$ bow and because its head is closest to the dark band interval at that wavelength. Only the positions and intensities of the $p = 6$ and $p = 7$ Airy maxima are shown in Fig. 2, ignoring other fainter rainbows. Evidently these positions of maxima change with both m and x. For example, by Eqs. (24a) and (24b) we further find that the $p = 6$ Airy maxima are inside (or closest to) the chosen test interval at the middle wavelength, $\lambda = 0.55\ \mu$m, which explains the highest contribution to the intensity by this rainbow, as seen in Fig. 6.

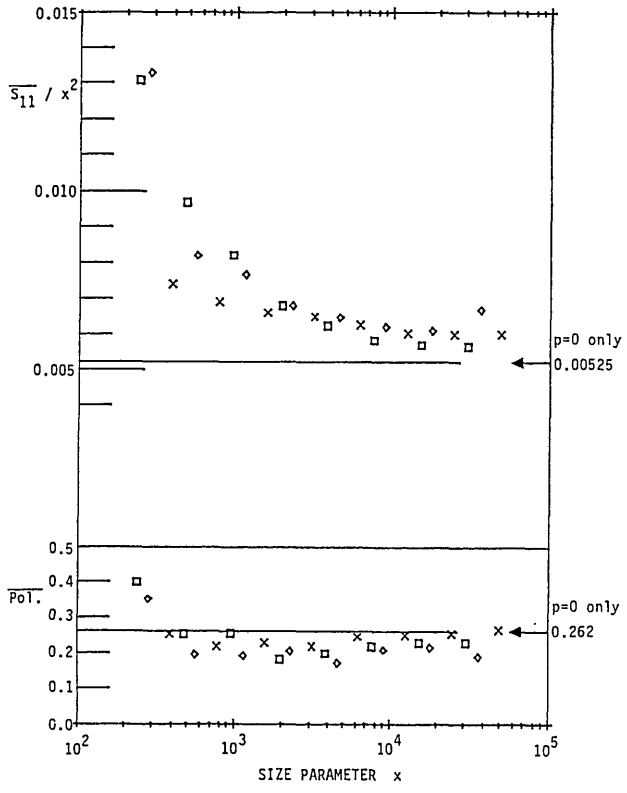

Fig. 6. Averaged S_{11}/x^2 and polarization over the chosen interval of $131° \le \theta \le 134°$ inside the dark band: ×, $\lambda = 0.40\ \mu$m, $m = 1.343 - i3E\text{-}9$; ◇, $\lambda = 0.55\ \mu$m, $m = 1.334 - i1.5E\text{-}9$; □, $\lambda = 0.65\ \mu$m, $m = 1.331 - i1.3E\text{-}8$.

At each size x we summed the individual contributions to the test interval by $p = 0$ GO rays and $p = 2$, 3, 6, and 7 Airy rainbows to compare with the Mie intensity. At small sizes the main rainbows ($p = 2$ and $p = 3$) spread into the test interval, while at large sizes only the $p = 6$ and $p = 7$ contributions persist. This explains the general downtrend seen in Fig. 6. The sums follow the Mie results fairly well (typically within ~10%) but come out a little too high at some large sizes, the worst case being ~22% off at $x = 30{,}933$ ($2a = 6.4$ mm drop at $\lambda = 0.65\ \mu$m). We checked by GO calculation that rays of different order did not affect these results, because their contributions (e.g., by $p = 5$ or $p = 10$) remained below 0.1% of the $p = 0$ contribution. The discrepancy is undoubtedly from the assumptions made in the Airy approximation. For example, by GO for $m = 4/3$ the $p = 6$ rays which reach the middle of the test interval, $\theta = 132.5°$, come from $\tau = 4.7°$ and 2.6°. Unlike the Airy theory assumptions, the values of ϵ_1^2 at these angles differ widely from each other and from the value at the GO rainbow ray incident angle. In a way it is surprising that the Airy approximation represents the actual $p = 6$ patterns so well. In conclusion, the crude adding of Airy intensities in the dark band cannot be expected to give perfect results. If a more

refined asymptotic theorty is needed, we recommend straight use of the Nussenzveig development.

V. Primary Rainbow Angle as a Key to Refractive Index and Size

Sunlit waterdrops are not the sole source of a rainbow phenomenon. Any transparent spherical particle, much larger than the wavelength, produces rainbows in particular directions. As seen in Eqs. (24a)–(24c) the rainbow angles depend most critically on refractive index m and the number of internal reflections, $p - 1$, but also to some degree on drop size x. The rainbow angle, computed either from Mie theory or the Airy approximation, may prove to be a powerful tool in characterizing a particle.

The practicality of this suggestion may be assessed from Fig. 7, where Mie and Airy rainbow profiles are compared by choosing a fixed size, $x \sim 242$, and four values of the refractive index. They correspond to (1) xylene in water being illuminated by He–Ne laser ($\lambda = 0.4747$ μm in water) [Fig. 7(a)], (2) water at 0.65 μm [Fig. 7(b)], (3) CO_2 ice at 0.679 μm [Fig. 7(c)], and (4) silicate at 0.50 μm [Fig. 7(d)]. The respective values for m are from Refs. 31, 36, 40, and 41, and the actual particle diameters are 36.5, 50, 52.2, and 38.5 μm. All the particles are of appropriate size for easy laboratory levitation and Mie calculations. Airy pattern evaluation is far simpler than Mie's but both can be carried out with an inexpensive computer, such as our PDP 11/23.

We first note that at this rather small x the first maximum of the primary rainbow ($p = 2$) still fits the Airy approximation both in position and intensity, for all four m terms. As m increases, so does the brightness of this peak, and for the highest two refractive indices [Figs. 7(c) and (d)], also the contrast. At the same time the agreement between the two theories in peak position is seen to improve.

Whenever we go to the supernumeraries for $p = 2$ or to the rainbows of higher order ($p \geq 3$), the agreement between the Mie and Airy theories becomes less impressive or is virtually lost at the sizes of Fig. 7. Test runs at a still smaller size, $x \sim 121$, show that the Airy approximation was still useful in identifying the main ($p = 2$) rainbow peak for $m > 4/3$.

VI. Conclusion

The art of making reliable Mie computations has been steadily improving. Owing to the combined efforts of many authors over many years such computations can now be made up to $x \sim 50{,}000$, at least. The comparison (Appendix A) of our ratio method (Sec. II) with three other codes shows that our algorithm ranks among the best. Due to its stability only a modest number of digits is required in the algorithm. With an eight-digit single precision calculation by VAX 11/750, for example, the detailed scattering from an $m \sim 4/3$ drop can be evaluated over $0.0001 \leq x \leq 25{,}000$.

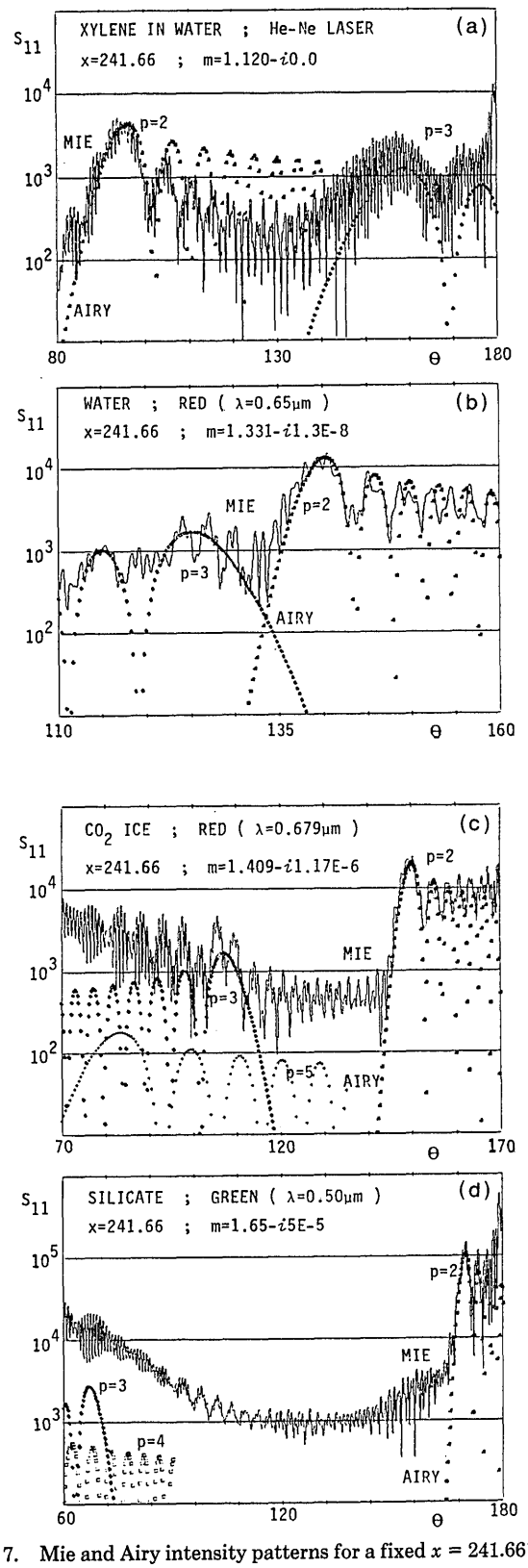

Fig. 7. Mie and Airy intensity patterns for a fixed $x = 241.661$ and four refractive indices.

We deliberately chose to compare the Mie computation with Airy's theory, which is a simple asymptotic

theory valid for large drop sizes. We found that, contrary to what has often been thought, but in agreement with conclusions reached earlier[33] for the $p = 2$ rainbow only, the Airy theory starts to be useful at relatively small sizes. For a drop size of 0.1 mm it already represents the main maxima of the primary ($p = 2$) and secondary ($p = 3$) rainbows quite well. At larger sizes, as illustrated by graphs for diameters of 0.4 and 3.2 mm, the agreement is excellent in position, intensity, and polarization of the main peak and many supernumerary maxima. A slight spread in sizes helps to bring out the agreement by suppressing irrelevant interference wiggles. Test runs for even smaller sizes (Sec. V) and various refractive indices showed that the first peak of the main ($p = 2$) rainbow is still well represented by the Airy theory. The agreement improves with increasing refractive index.

Finer detail was tested by examining the dark band between the main rainbows, where (at the largest size illustrated) the intensity drops below 0.5% of that in

Table I. Comparison of the Numerical Data for Four Mie Codes

Author		Dave[18]	Bohren & Huffman[14]*	Shah[21]	Wang this paper
Code		DBMIE	BHMIE	MIEHISS	VXMX1D
Non-absorbing refractive index m:					
x=0.0001	Qext	2.3068E-17	2.3068E-17		2.3068E-17
m=1.50	Qabs	0.0	0.0		0.0
	Qback	3.4602E-17	3.4602E-17		3.4602E-17
x=5.21282	Qext	3.10542	3.10543	3.10542	3.10543
m=1.55	Qabs	0.0	0.0	0.0	0.0
	Qback	2.92534	2.92534	2.92534	2.92534
x=100*	Qext	2.0944	2.0944	2.0944	2.0944
m=1.50	Qabs	0.0	0.0	0.0	0.0
	Qback	1.7362	1.7367	1.7362	1.7362
x=1570.7963	Qext	2.01294		2.01294	2.01294
m=1.342	Qabs	0.0		0.0	0.0
	Qback	1.769555		1.771846	1.769558
x=25000	Qext	2.00235		2.00235	2.00235
m=1.50	Qabs	0.0		0.0	0.0
	Qback	123.8323		123.8615	123.8322
Absorbing refractive index m:					
x=0.0001	Qext	1.9925E-5	1.99252E-5	1.9925E-5	1.9925E-5
m=1.50 - *i* 0.1	Qabs	1.9925E-5	1.9925E-5	1.9925E-5	1.9925E-5
	Qback	3.60336E-17	3.60336E-17	3.6034E-17	3.6034E-17
x=5.21282	Qext	2.86165	2.86165	2.86165	2.86165
m=1.55 - *i* 0.1	Qabs	1.19740	1.19740	1.19740	1.19740
	Qback	0.205995	0.205995	0.205995	0.205995
x=100*	Qext	2.0898	2.0898	2.0898	2.0898
m=1.50 - *i* 0.1	Qabs	0.9577	0.9577	0.9577	0.95769
	Qback	0.04153	0.04153	0.04153	0.04153
x=1570.7963	Qext	2.01445		2.01445	2.01445
m=1.342 - *i* 0.1	Qabs	0.93354		0.93354	0.93354
	Qback	0.023106		0.023106	0.023106
x=25000	Qext	2.00232		2.00232	2.00232
m=1.50 - *i* 0.1	Qabs	0.90641		0.90641	0.90641
	Qback	0.041533		0.041534	0.041534

* BHMIE is in single-precision (SP) arithmetic. All efficiencies for x=100 are computed using 7-digit SP arithmetic of PDP 11/23 computer. Others except BHMIE are by 16-digit double-precision calculations via VAX 11/750.

the primary Airy peak. In this dark band the externally reflected light ($p = 0$) and the rainbows for $p = 6$ and $p = 7$, which shift rapidly with wavelength, explain most of the intensity. The $p = 6$ bow matches its Airy pattern surprisingly well.

The Mie algorithm analysis was generally confirmed by computing the glare points.[42] In this technique, which we shall publish separately, the Mie routine is complemented by a lens that makes an image of the drop as viewed from a finite distance at various scattering directions.

The overall conclusion is that over a wide size range Airy's theory gives simple, reliable answers, which may be useful, e.g., in diagnosing the characteristics of particles in laboratory experiments or in astronomy. If a more refined theory is needed, we recommend either straight Mie computations or the full asymptotic theory of Nussenzveig.

We thank J. L. Weinberg, president of the ISST, for supporting our collaboration. R. T. Wang's work was supported in part by the U.S. Army Research Office under contract DAAL03-86-K0021 to the University of Florida where this work was initiated.

Appendix A: Accuracy and Speed Comparisons Using Four Mie Codes

Accuracy and speed via our ratio Mie codes are compared with those by Dave's DBMIE,[18] Bohren-Huffman's BHMIE[14] and Shah's MIEHISS.[21] The last three codes by other authors were duplicated or edited for use in the VAX 11/750 double precision (DP, sixteen

Table II. CPU Time t in Seconds by Four Mie Codes* Using Single Precision Arithmetic (Seven Digits) on the DECLAB PDP 11/23 Computer

	Author	Dave		Bohren-Huffman		Shah		Wang	
	$x=2\pi a/\lambda$	t	n_{max}	t	n_{max}	t	n_{max}	t	n_{max}
		m=1.50 - i 0.0							
Evaluating Mie coefficients only	.1	.137	3	.212	3	.462	3	.162	4
	5.2	.445	15	.535	14	.675	11	.400	13
	100.	3.75	121	3.75	120	3.65	115	3.60	120
	250.	(8.75	278)	8.55	277	9.10	269	8.40	277
	500.	(16.8	534)	16.5	533	15.4	522	16.2	531
		m=1.50 - i 0.10							
	.1	.174	3	.267	3			.207	4
	5.2	.560	15	.680	14	1.01	15	.510	13
	100.	4.75	121	4.85	120	5.05	124	4.55	119
	250.	(11.05	278)	11.10	277	10.50	281	10.70	276
	500.	(21.4	534)	21.4	533	19.7	538	20.8	533
		m=1.50 - i 0.0, $0°\le\theta(1°)\le180°$							
Computing all efficiencies and Müller matrix elements	100.	240		306		247		256	
	250.	(544)		723		569		581	
		m=1.50 - i 0.10, $0°\le\theta(1°)\le180°$							
	100.	243		307		267		255	
	250.	(549)		725		596		581	
		m=1.331 - i 1.3 E-8, $110°\le\theta(0.1°)\le160°$							
	241.661					1508		1520	

*All codes are translated by Wang from the original authors. n_{max} denotes the Mie series termination. The SP-edited Dave's DBMIE developed numerical instabilities during the bracketted calculations.

digits) and PDP 11/23 single precision (SP, seven digits) calculations, and checked to agree with their published results. Use of the PDP 11/23 is also to determine the practicality of the codes. We thank G. A. Shah of the Indian Institute of Astrophysics, Bangalore, India, for providing his code and the recent numerical tabulation which had been tested to agree with Wiscombe's[15] result for $x \leq 1000$ and $x = 5000$.

1. Accuracy

Table I compares the Q_{ext}, Q_{abs}, and Q_{back}, the extinction, absorption, and backscatter efficiencies, which are the easiest to show the Mie coefficients accuracy. All the codes except BHMIE were originally in DP arithmetic, hence only the $x = 100$ values are by the PDP 11/23 SP calculation, the rest being by the VAX DP. It is seen that all the codes give excellent agreement over the entire tabulated range of x. Note in particular that Q_{back} for $x = 100$ and $m = 1.5 - i0.1$ has already reached the geometrical optics limit given by Bohren-Huffman (Ref. 14, p. 123).

All four codes have been translated or edited for SP calculation by the PDP 11/23, thereby generating all Mie coefficients, efficiencies, asymmetry factors, and Müller matrix elements. DBMIE cannot be used for the purpose without substantial modification, and we edited it by imposing Eqs. (3) and (7) on his algorithm, among several other editings. Otherwise, Q_{back} diverged when $x \gtrsim 170$ and numerical instabilities developed when $x \lesssim 0.01$. When only Q_{ext} and Q_{abs} are concerned, however, we found that all four codes agreed with each other to ~5 figures for x as large as $x = 500$, although nonzero Q_{abs} was seen to creep into the fifth decimal place in BHMIE output for $m'' = 0$ at $x = 500$. Besides Q_{back}, we found that the Müller matrix element S_{34} was most sensitive to change in x and m, and hence a good indicator for accuracy. Our ratio Mie codes, written both in SP and DP arithmetic, were also compared with each other, using both the VAX and PDP computers. With the VAX computer, it was gratifying to find that even when the water drop reached $x \sim 25000$, both the SP (eight digits) and DP results agreed at least to the fourth significant figure for Q_{ext} and Q_{abs}, and to the second figure for $(S_{11})_{Mie}$ and $(P)_{Mie}$. Similar accuracy was maintained even with the PDP SP calculation to x ~600 (near to exhausting the available 68K memory). Hence, for many practical applications the ratio algorithm does not require double precision computation.

2. Speed

The CPU times for computing complete single particle scattering matrices were found proportional to sphere size x and the number of scattering angles (typically 10^{-3} s/angle $\gtrsim 180$). For our ratio codes they are (1) $\sim 0.23 \cdot x \cdot 10^{-3}$/angle by the VAX DP calculation, (2) $\sim 0.12 \cdot x \cdot 10^{-3}$ s/angle by the VAX SP calculation, and (3) $12.6 \cdot x \cdot 10^{-3}$ s/angle by the PDP SP calculation. For case (1), our DP code VXMX1D was found ~1.6 times faster than DBMIE for computing all the efficiencies.

Table II shows the CPU time comparison for the four Mie codes in Table I, all translated/edited for PDP 11/23 single precision calculation. We note that there are no substantial gains in speed by using the ratio method for these medium or small sized particles. However, the numerical stability even by SP calculation for large x may prove to be the most efficient method for calculation of scattering by size distribution drops. It will be interesting to see if the codes can be vector structured as Wiscombe's algorithm.[15]

References

1. L. V. Lorenz, "Upon the Light Reflected and Refracted by a Transparent Sphere," Vidensk. Selsk. Shrifter **6**, 1–62 (1890), in Danish. Reference sources: N. A. Logan, "Survey of Some Early Studies of the Scattering of Plane Waves by a Sphere," in *Proceedings, Second International Congreee on Optical Particle Sizing*, E. D. Hirleman, Ed. (Arizona State U.P., Tempe, 1990), pp. 7–15; H. Kragh, "Ludvig V. Lorenz and His Contributions to Light Scattering," in *Proceedings, Second International Congress on Particle Sizing*, E. D. Hirleman, Ed. (Arizona State U.P., Tempe, 1990), pp. 1–6.
2. G. Mie, "Beitrage zur Optik trüber Medien, speziell kolloidaler Metallosungen," Ann. Phys. Leipzig **25**, 377–445 (1908).
3. P. Debye, "Der Lichtdruck auf Kugeln von beliebigem Material," Ann. Phys. Leipzig **30**, 57–136 (1909).
4. B. van der Pol and H. Bremmer, "The Diffraction of Electromagnetic Waves from an Electrical Point Source Round a Finitely Conducting Sphere, with Applications to Radio–Telegraphy and the Theory of the Rainbow," Philos. Mag. **24**, 141–176, 825–864 (1937); **25**, 817–837 (1938).
5. C. B. Boyer, *The Rainbow: from Myth to Mathematics* (Yoseloff, New York, 1959).
6. H. M. Nussenzveig, "The Theory of the Rainbow," Sci. Am. **236**, 116–127 (1977).
7. A. B. Fraser, "Chasing Rainbows," Weatherwise **36**(6), 280–289 (1983); "Why can the Supernumerary Bows be Seen in a Rain Shower?," J. Opt. Soc. Am. **73**, 1626–1628 (1983).
8. M. Minnaert, *The Nature of Light and Color in the Open Air* (Dover, New York, 1954).
9. R. Greenler, *Rainbows, Halos, and Glories* (Cambridge U.P., New York, 1980).
10. H. C. van de Hulst, *Light Scattering by Small Particles* (Wiley, New York, 1957).
11. H. M. Nussenzveig, "High-Frequency Scattering by a Transparent Sphere. I. Direct Reflection and Transmission," J. Math. Phys. New York **10**, 82–124 (1969); II. Theory of the Rainbow and the Glory," J. Math. Phys. New York **10**, 125–176 (1969).
12. V. Khare and H. M. Nussenzveig, "Theory of the Rainbow," Phys. Rev. Lett. **33**, 976–980 (1974); "The Theory of the Glory," in *Statistical Mechanics and Statistical Methods in Theory and Application*, U. Landman, Ed. (Plenum, New York, 1977), pp. 723–764.
13. H. M. Nussenzveig, "Complex Angular Momentum Theory of the Rainbow and the Glory," J. Opt. Soc. Am. **69**, 1068–1079 (1979); see also p. 1193, plate 107.
14. C. F. Bohren and D. R. Huffman, *Absorption and Scattering of Light by Small Particles* (Wiley, New York, 1983).
15. W. J. Wiscombe, "Mie Scattering Calculations: Advances in Technique and Fast, Vector-Speed Computer Codes," NCAR (Natl. Ctr. Atmos. Res.) Tech. Note 140+STR (1979); "Improved Mie Scattering Algorithms," Appl. Opt. **19**, 1505–1509 (1980).
16. M. Kerker, *The Scattering of Light and Other Electromagnetic Radiation* (Academic, NewYork, 1969).

17. G. W. Kattawar and G. N. Plass, "Electromagnetic Scattering from Absorbing Spheres," Appl. Opt. **6,** 1377–1382 (1967).
18. J. V. Dave, "Subroutines for Computing the Parameters of Electromagnetic Radiation Scattered by a Sphere," Report 320-3237, IBM Scientific Center, Palo Alto, CA (1968); "Scattering of Visible Light by Large Water Spheres," Appl. Opt. **8,** 155–164 (1969).
19. D. Deirmendjian, *Electromagnetic Scattering on Spherical Polydispersions* (Elsevier, New York, 1969).
20. W. J. Lentz, "Generating Bessel Functions in Mie Scattering Calculations Using Continued Fractions," Appl. Opt. **15,** 668–671 (1976).
21. G. A. Shah, "Numerical Methods for Mie Theory of Scattering by a Sphere," Kodaikanal Obs. Bull. Ser. A **2,** 42–63 (1977); "Numerical Evaluation of Spherical Bessel and Related Functions," Kodaikanal Obs. Bull. Ser. A **3,** 107–119 (1983); private communication (1989).
22. A. Ungut, G. Grehan and G. Gouesbet, "Comparisons Between Geometrical Optics and Lorentz-Mie Theory," Appl. Opt. **20,** 2911–2918 (1981).
23. W. A. Rooij and C. C. A. H. van der Stap, "Expansion of Mie Scattering Matrices in Generalized Spherical Functions," Astron. Astrophys. **131,** 237–248 (1984).
24. D. W. Schuerman, R. T. Wang, B. A. S. Gustafson and R. W. Schaefer, "Systematic Studies of Light Scattering. 1: Particle Shape," Appl. Opt. **20,** 4039–4050 (1981).
25. R. T. Wang and W. X. Wang, "Scattering by Arbitrarily Large Homogeneous/Concentric Spheres—Exact Theory with Use of New Efficient Algorithms," in *Proceedings of the 1985 Scientific Conference on Obscuration and Aerosol Research*, R. Kohl, Ed. (Army CRDEC-SP-86019, Aberdeen, MD 1986), pp. 381–409.
26. R. T. Wang, "A New Algorithm for Exact Scattering Calculations Using Ratios," submitted to *Proceedings of the 1988 Scientific Conference on Obscuration and Aerosol Research*, Army CRDEC, Aberdeen, MD.
27. G. B. Airy, "On the Intensity of Light in the Neighborhood of a Caustic," Trans. Cambridge Philos. Soc. **6,** 379–402 (1838).
28. This notation, taken from Ref. 10, has the advantage of making superfluous a separate notation for the externally reflected ray ($p = 0$) and the directly transmitted ray ($p = 1$). We comply with common practice of calling $p - 1$ the order of rainbow.
29. W. J. Humphreys, *Physics of the Air* (McGraw-Hill, New York, 1929).
30. M. Abramowitz and I. A. Stegun, Eds, *Handbook of Mathematical Functions* (Dover, New York, 1964).
31. P. L. Marston, "Rainbow Phenomena and the Detection of Nonsphericity in Drops," Appl. Opt. **19,** 680–685 (1980).
32. K. Sassen, "Angular Scattering and Rainbow Formation in Pendant Drops," J. Opt. Soc. Am. **69,** 1083–1089 (1979).
33. J. H. Saiac, "Etude de la diffusion de la lumiere par les gouttes d'eau dans le phenomene de l'arc en ciel," La Meteorologie **16,** 29–68 (1970).
34. C. W. Querfeld, "Mie Atmospheric Optics," J. Opt. Soc. Am. **55,** 105–106 (1965).
35. J. A. Lock, "Theory of the Observations Made of High-Order Rainbows from a Single Water Droplet," Appl. Opt. **26,** 5291–5298 (1987).
36. W. M. Irvine and J. B. Pollack, "Infrared Optical Properties of Water and Ice Spheres," Icarus **8,** 324–360 (1968).
37. J. E. Hansen and L. D. Travis, "Light Scattering in Planetary Atmospheres," Space Sci. Rev. **16,** 527–610 (1974).
38. J. V. Dave, "Effect of Coarseness of the Integration Increment on the Calculation of the Radiation Scattered by Polydispersed Aerosols," Appl. Opt. **8,** 1161–1167 (1969).
39. J. D. Walker, "How to Create and Observe a Dozen Rainbows in a Single Drop of Water," Sci. Am. **237,** 138–144 (1977); "Mysteries of Rainbows, Notably Their Rare Supernumerary Arcs," Sci. Am. **242,** 147–152 (1980); "Multiple Rainbows from Single Drops of Water and Other Liquids," Am. J. Phys. **44,** 421–433 (1976).
40. S. G. Warren, "Optical Constants of Carbon Dioxide Ice," Appl. Opt. **25,** 2650–2673 (1986).
41. D. R. Huffman and J. L. Stapp, "Interstellar Extinction Related to 2200Å Band," Nature London Phys. Sci. **229,** 45–46 (1971).
42. H. C. van de Hulst and R. T. Wang, "Glare Points," in *Proceedings, Second International Congress on Optical Particle Sizing*, E. D. Hirleman, Ed. (Arizona State U.P., Tempe, 1990), pp. 40–49.